Methods for Diffusive Relaxation in the P_N Equations[‡]

Cory D. Hauck[*], Robert B. Lowrie[†], Ryan G. McClarren[†]

Los Alamos National Laboratory
Computational Physics Group (CCS-2)
Los Alamos, New Mexico 87544 USA

Abstract

We present recent progress in the development of two substantially different approaches for discretizing the P_N equations. These equations form a linear hyperbolic system that may be used to model particle transport in a material medium, and in highly collisional regimes, their solution can be accurately approximated by the solution of a simple diffusion equation. This approximation is based on a balance between function values and gradients of certain variables in the P_N system. Conventional high-resolution schemes, based on variable reconstruction methods, approximate such gradients with an error that is dependent on the size of the computational mesh. Thus in order to capture the diffusion limit, a given mesh must resolve the dynamics of the continuum equation at the level of the mean-free-path, which tends to zero in the diffusion limit.

The two methods analyzed here produce accurate solutions in both collisional and non-collisional regimes; in particular, they do not require resolution of the mean-free-path in order to properly capture the diffusion limit. The first method is a straightforward application of the discrete Galerkin (DG) methodology, which uses additional variables in each computational cell to capture the balance between function values and gradients, which are computed locally. The second method uses a temporal splitting of the fast and slow dynamics in the P_N system to derive so-called *regularized equations* for which the diffusion limit is built-in.

We focus specifically on the P_N equations for one-dimensional, slab geometries. Preliminary results for several benchmark problems are presented which highlight the advantages and disadvantages of each method. Further improvements and extensions are also discussed.

1 Introduction

This study will investigate several numerical methods for modeling the transfer of neutral particles through a material medium, such as neutrons within a nuclear reactor. In a kinetic

[*]also Center for Nonlinear Studies (CNLS), Mail Stop B258.

[†]Mail Stop D413.

[‡]Los Alamos Report, LA-UR-08-04966. Work supported by the U.S. Department of Energy at Los Alamos National Laboratory under contract DE-AC52-06NA25396. The first author also gratefully acknowledges the support of the DOE Office of Science Advanced Computing Research (ASCR) Program.

description, the particle evolution is governed by a transport equation, generally of the form

$$\partial_t F + v \cdot \nabla_x F = \mathcal{C}(F)\,. \tag{1}$$

Here $x \in \Omega \subset \mathbb{R}^3$ is a spatial coordinate, $v \in \mathbb{R}^3$ is a velocity coordinate, $t \geq 0$ is time, and the function $F = F(x, v, t)$ is the non-negative distribution of particles in position-velocity phase space. The left-hand side of (1) describes the evolution of F along inertial trajectories, while the collision operator $\mathcal{C}$ on the right-hand side describes particle interactions with the medium via scattering and absorption/emission processes.

Typically, there exists a diffusion limit for (1) in which F is approximated by a non-negative scalar function of space and time that satisfies a standard diffusion equation. This approximation is valid when collision processes dominate, i.e., when the mean free path between collisions is small compared to macroscopic variations in the system. Because collisions drive particles into equilibrium with the surrounding medium, long time scales (relative to the collision process) are required in order to observe diffusion dynamics.

A common approach to solving (1) is with moment methods. In the moment approach, one tracks the evolution of a finite number of velocity moments of F. These moments, which are functions of space and time only, can then be used to reconstruct an approximation of F. Their evolution is approximated by a system of partial differential equations that are derived directly from (1). The exact form of these equations and the reconstruction of F is known as the *closure problem*. A basic requirement of any closure is that the resulting moment system has the same diffusion limit as the transport equation (1).

Moment equations play an important role in so-called *transition regimes*, where collisions are frequent enough to impose macroscopic structure onto a particle system, but not frequent enough to validate the diffusion limit. Roughly speaking, as the number of particle interactions decreases, the system becomes less organized and more moments will be needed for an accurate approximation of F. Thus simulations of multiscale transport phenomena can use moment equations in three fundamental ways:

- As stand-alone models, with the flexibility to improve accuracy by adding more moments;
- As preconditioners for more complicated models that may suffer from numerical stiffness;
- In hybrid schemes that select components from a hierarchy of models in such a way as to maximize efficiency for a given level of accuracy. Thus expensive, high-resolution models are used only in regimes where they are needed.

For numerical simulations, the hyperbolic nature of many moment systems and the parabolic nature of the diffusion approximation are not always compatible. In such cases, the simulation of multi-scale problems with multiple temporal and spatial scales can be a challenge. In practice, there is a need for hyperbolic solvers that can handle shocks and discontinuities associated with streaming regimes (when the collisions are less frequent), but also behave like standard diffusion solvers in diffusive regimes. In particular, a hyperbolic solver should, in a specific asymptotic limit, reduce to a discretization of the relevant diffusion equation. This is the so-called *asymptotic preserving property* [26]. Unfortunately,

hyperbolic solvers use numerical dissipation to capture discontinuities, and unless formulated carefully, this dissipation increases as the system approaches the diffusion limit. At some point, the numerical dissipation dominates the actual physical diffusion in the system. Consequently, one may generate results which appear very well resolved, but are far from accurate.

Another drawback of conventional hyperbolic solvers is a restrictive time step. In diffusive regimes, the relevant time scales are related to the macroscopic features of the system. However, hyperbolic solvers typically take time steps on the order of the (much smaller) particle mean flight time in order to maintain stability. As a result, the simulation of diffusive systems with hyperbolic solvers is often inefficient.

In the present paper, we focus our attention on the P_N *equations* [36, 51], for which the reconstruction of F is a finite, linear combination of Legendre polynomials in the velocity variable with coefficients that depend on space and time. Here the letter 'P' is the conventional notation for these polynomials and the integer N refers to the order of the expansion. When $N = 1$, the P_N equations are equivalent to the *hyperbolic heat equation* [49,12,11,23].

2 Neutron Transport

We consider a simple model for neutron transport with the following assumptions:

1. Particles travel in different directions, but the speed $|v|$ (and hence the particle energy) is assumed to be fixed.

2. The material medium is defined on a one-dimensional, "slab" geometry. Consequently, the distribution of neutrons is a function of time (t), a single spatial coordinate (x), and the angular coordinate $\mu \in [-1, 1]$, where μ is the direction cosine of the particle trajectory.

3. Particles interact with the medium only through scattering that is isotropic, i.e., independent of μ.

2.1 The Transport Equation

In the neutron transport community, the fundamental quantity of interest in the kinetic description is the *angular flux* $\psi(x, \mu, t)$ which, in the context of our simplified model, is related to the phase-space density $F(x, \mu, t)$ by the simple relation $\psi = |v|F$. In particular, the integral

$$\int_{-1}^{1} \mu\psi(x_0, \mu, t)\, d\mu \tag{2}$$

gives the flux of particles across the plane $x = x_0$. Under the assumptions of our simplified model, the transport equation (1) for ψ is

$$\frac{1}{|v|}\partial_t\psi + \mu\partial_x\psi = -\sigma_{\mathrm{s}}\left(\psi - \frac{1}{2}\langle\psi\rangle\right), \tag{3}$$

where the *scattering cross-section* $\sigma_{\rm s}(x) > 0$ is the inverse of the mean free path between scattering events and, for any measurable function $g = g(\mu)$,

$$\langle g \rangle \equiv \int_{-1}^{1} g(\mu) d\mu \, . \tag{4}$$

2.2 Comments on Generalizations

There are several physically meaningful generalizations to (3). For completeness, we will briefly describe some of these generalizations and refer the reader to one of several monographs [6, 10, 36] for further discussion. These generalizations include:

Non-isotropic Scattering. It is possible to model scattering processes that have a preferred direction (non-isotropic scattering) by making the following replacement on the right-hand side of (3):

$$\frac{\sigma_{\rm s}}{2}\langle \psi \rangle \mapsto \sigma_{\rm s} \int_{-1}^{1} \omega(\mu' \to \mu) \psi(\mu') \, d\mu' \, , \tag{5}$$

where $\omega(\mu' \to \mu)$ is the probability that a scattering event will change a neutron's direction of travel from μ' to μ. Thus in (3), we have set $\omega = 1/2$.

Absorption. It is also possible for a neutron to be absorbed by the material medium. To model such situations, the right-hand side of (3) is replaced by

$$-\sigma_{\rm s} \left(\psi - \frac{1}{2}\langle \psi \rangle \right) \mapsto -(\sigma_{\rm a} + \sigma_{\rm s})\psi - \frac{\sigma_{\rm s}}{2}\langle \psi \rangle \, , \tag{6}$$

where the absorption cross-section $\sigma_{\rm a}(x)$ is defined as the inverse of the average distance a neutron travels in the particular material medium before undergoing an absorbing collision.

Fission. In a fission process, neutrons separate atoms in the material medium, which consequently release additional neutrons. This process can be modeled by replacing the right-hand side of (3) with

$$-\sigma_{\rm s} \left(\psi - \frac{1}{2}\langle \psi \rangle \right) \mapsto -(\sigma_{\rm a} + \sigma_{\rm s} + \sigma_{\rm f})\psi - \frac{\sigma_{\rm s} + \nu\sigma_{\rm f}}{2}\langle \psi \rangle \, , \tag{7}$$

where $\sigma_{\rm f}(x, t)$ is the fission cross-section and the multiplier $\nu > 0$ is the average number of neutrons released per fission reaction.

General Spatial Domains. Equation (3) treats only neutron distributions that vary in one spatial dimension. However, in practice, more complex curvilinear and fully three dimensional geometries are also considered.

Multiple Speeds. In practice, neutrons do not move with a fixed speed $|v|$. Indeed, collision events often induce an exchange of energy between neutrons and the material medium, in what is referred to as *non-coherent scattering*. In such cases, ψ and the cross-sections become functions of the neutron energy as well as angle. However, the energy dependence of ψ is most commonly treated with a multigroup approximation in which the transport equation is solved for specific ranges of the energy [36]. These ranges are carefully selected in order to capture spikes in the neutron energy spectrum that are a result of resonances in the cross-sections and cannot be accurate modeled using the moment approach.

These generalizations, although important for many practical problems, are not necessary for our initial studies. Indeed, the fundamental numerical challenges of modeling diffusive relaxation for neutron transport can be addressed using the simplified form given by (3).

2.3 Scalings and the diffusion limit

The transport equation (3) has a well-known diffusion limit in which ψ is approximated by its angular average $\phi := \langle \psi \rangle$, known as the *scalar flux*, and the evolution of ϕ is approximated well by a simple diffusion equation.

To derive the diffusion limit, we begin by re-expressing the transport equation (3) in terms of the following dimensionless variables for time, space, and cross-section:

$$\hat{x} := \frac{x}{x_0}\,, \qquad \hat{t} := \frac{t}{t_0}\,, \qquad \hat{\sigma}_{\mathrm{s}} := \frac{\sigma_{\mathrm{s}}}{\sigma_0}\,. \tag{8}$$

Here x_0 and t_0 are macroscopic scales for space and time and σ_0 is a representative value of the cross-section. When expressed in terms of the dimensionless parameters

$$\varepsilon := \frac{1}{x_0 \sigma_0} \qquad \text{and} \qquad \delta := \frac{x_0}{t_0 v}\,, \tag{9}$$

the transport equation (3) takes the dimensionless form

$$\delta \partial_{\hat{t}} \hat{\psi} + \mu \partial_{\hat{x}} \hat{\psi} = -\frac{\hat{\sigma}_s}{\varepsilon} \left(\hat{\psi} - \frac{1}{2} \langle \hat{\psi} \rangle \right)\,, \tag{10}$$

where $\hat{\psi}(\hat{x}, \mu, \hat{t}) := \psi(x, \mu, t)$. The reader may note that the parameters ε and δ correspond to the Knudsen number [13] and kinetic Strouhal number [20,57], respectively, both of which are used in the kinetic theory of dilute gases.

The diffusion scaling for the transport equation comes from setting $\delta = \varepsilon$ in (10) so that (removing hats)

$$\varepsilon \partial_t \psi + \mu \partial_x \psi = -\frac{\sigma_{\mathrm{s}}}{\varepsilon} \left(\psi - \frac{1}{2} \langle \psi \rangle \right)\,. \tag{11}$$

Equation (11), which we will refer to as the *scaled transport equation*, will serve as the foundation for all derivations and analysis in the remainder of this manuscript.

Associated with (11) is the following conservation law for ϕ:

$$\varepsilon \partial_t \phi + \partial_x \langle \mu \psi \rangle = 0\,. \tag{12}$$

For $\varepsilon \ll 1$, one can formally derive a closure for (12) using a Chapman-Enskog expansion[1], by formally expanding ψ in powers of ε:

$$\psi = \psi^{(0)}[\phi] + \varepsilon\psi^{(1)}[\phi] + \varepsilon^2\psi^{(2)}[\phi] + \dots \,. \tag{13}$$

Substituting (13) into (11) and equating powers of ε gives

$$\psi = \frac{1}{2}\phi - \frac{\varepsilon\mu}{\sigma_{\mathrm{s}}}\partial_x\phi + O(\varepsilon^2)\,, \tag{14}$$

and plugging (14) back into (12) shows that ϕ satisfies the diffusion equation

$$\partial_t\phi = \partial_x\left(\frac{1}{3\sigma_{\mathrm{s}}}\partial_x\phi\right)\,, \tag{15}$$

up to an $O(\varepsilon)$ error. In fact, one can show further that (15) is formally accurate up to $O(\varepsilon^2)$ [48].

The Chapman-Enskog analysis can be carried out to arbitrary order. For example

$$\psi^{(2)} = \left(\frac{1}{2}\mu^2 - \frac{1}{6}\right)\partial_x^2\rho\,, \tag{16}$$

$$\psi^{(3)} = \left(-\frac{1}{2}\mu^3 + \frac{1}{3}\mu\right)\partial_x^3\rho\,, \tag{17}$$

$$\psi^{(4)} = \left(\frac{1}{2}\mu^4 - \frac{1}{2}\mu^2 + \frac{1}{15}\right)\partial_x^4\rho\,, \tag{18}$$

$$\psi^{(5)} = \left(-\frac{1}{2}\mu^5 + \frac{2}{3}\mu^3 - \frac{17}{90}\mu\right)\partial_x^5\rho\,, \tag{19}$$

and

$$\partial_t\rho = \frac{1}{3}\partial_x^2\rho - \frac{1}{45}\varepsilon^2\partial_x^4\rho + \frac{2}{945}\varepsilon^4\partial_x^6\rho + O(\varepsilon^6)\,. \tag{20}$$

However, these higher-order approximations prove less useful and the specification of the additional, required boundary conditions is difficult.

3 The P_N Equations

The P_N equations are linear moment equations that are derived by expanding ψ in the variable μ as a linear combination of spherical harmonic polynomials. The unknowns in the P_N system are (up to a linear transformation) the coefficients of this expansion. In our one-dimensional setting, the spherical harmonics polynomials are just the Legendre polynomials on the interval $[-1, 1]$, and the P_N equations form a set of $N + 1$ linear hyperbolic balance laws.

Because the P_N equations are linear, they suffer from two major drawbacks. First, the wave speeds of the P_N system are constant and always underestimate the speed of information

[1]The diffusion limit can also be derived via Hilbert expansion. See, for example, [55].

flow (although see [15]). Second, the linear expansion of ψ can take on negative values, even though ψ itself is an inherently non-negative quantity. In spite of these drawbacks, the P_N equations are a valuable tool for studying the asymptotic behavior of more complicated nonlinear systems [47, 18, 8, 9]. In particular, they possess the basic features of diffusive relaxation and therefore serve as a prototype for nonlinear closures.

3.1 Derivation

If $\psi(x,\cdot,t) \in L^2(d\mu)$, then it can be expanded in terms of basis functions $\{p_n(\mu)\}_{n=0}^{\infty}$ defined on $\mu \in [-1,1]$:

$$\psi(x,\mu,t) = \sum_{n=0}^{\infty} v_n(x,t) p_n(\mu) \,. \tag{21}$$

By truncating this expansion at some positive integer N, substituting the truncation into (11), and then taking moments with respect to $\{p_n\}_{n=0}^{N}$, one can derive a system of equations which approximates the evolution of expansion coefficients $\{v_n\}_{n=0}^{N}$. With the vector notation

$$\mathbf{p} := (p_0, p_1, \ldots, p_N)^T \quad \text{and} \quad \mathbf{v} := (v_0, v_1, \ldots, v_N)^T \,, \tag{22}$$

these equations take the form

$$\left\langle \mathbf{p}\mathbf{p}^T \right\rangle \partial_t \mathbf{v} + \frac{1}{\varepsilon} \left\langle \mu \mathbf{p}\mathbf{p}^T \right\rangle \partial_x \mathbf{v} = -\frac{\sigma_s}{\varepsilon^2} \left(\left\langle \mathbf{p}\mathbf{p}^T \right\rangle - \frac{1}{2} \langle \mathbf{p} \rangle \langle \mathbf{p} \rangle^T \right) \mathbf{v} \,, \tag{23}$$

or in terms of the moments $\mathbf{u} = (u_0, u_1, \ldots, u_N)^T := \langle \mathbf{p}\psi \rangle = \left\langle \mathbf{p}\mathbf{p}^T \right\rangle \mathbf{v}$,

$$\partial_t \mathbf{u} + \frac{1}{\varepsilon} \left\langle \mu \mathbf{p}\mathbf{p}^T \right\rangle \left\langle \mathbf{p}\mathbf{p}^T \right\rangle^{-1} \partial_x \mathbf{u} = -\frac{\sigma_s}{\varepsilon^2} \left(\mathbf{u} - \frac{1}{2} \langle \mathbf{p} \rangle \langle \mathbf{p} \rangle^T \left\langle \mathbf{p}\mathbf{p}^T \right\rangle^{-1} \mathbf{u} \right) \,. \tag{24}$$

With a proper choice of basis, the right-hand side of (24) is usually much simpler than it appears in this general setting.

In the P_N approximation, the basis functions in (24) are the Legendre polynomials [3], which satisfy the orthogonality relation

$$\langle p_n p_m \rangle = \frac{2}{2n+1} \delta_{nm} \tag{25}$$

and the recursion relation

$$\mu p_n = \frac{n+1}{2n+1} p_{n+1} + \frac{n}{2n+1} p_{n-1} \,. \tag{26}$$

The first four Legendre polynomials are

$$p_0(\mu) = 1 \,, \quad p_1(\mu) = \mu \,, \quad p_2(\mu) = \frac{1}{2}\left(3\mu^2 - 1\right) \,, \quad p_3(\mu) = \frac{1}{2}(5\mu^3 - 3\mu) \,; \tag{27}$$

for notational convenience, we denote their corresponding moments by

$$\phi := u_0 \,, \quad J := u_1 \,, \quad P := u_2 \,, \quad q := u_3 \,. \tag{28}$$

The definition of the scalar flux ϕ above is consistent with the previous definition in the beginning of Section 2.3. The variables J and P are usually referred to as the *current* and *pressure*, respectively. These terms are standard in the nuclear engineering literature, though the astrophysics community uses different notation and terminology [46, 51]. The variable q does not commonly carry a name. However, in the context of moment equations, it is mathematically similar to the heat flux in the kinetic theory of gases (which explains the notation used here.)

Using (25) and (26) and the fact that $p_0 = 1$, one can evaluate the integrals in (24) to arrive at the (scaled) P_N equations

$$\partial_t \mathbf{u} + \frac{1}{\varepsilon}(A + B)\,\partial_x \mathbf{u} = -\frac{\sigma_s}{\varepsilon^2} Q\mathbf{u}\,, \tag{29}$$

where the flux matrices A and B and the relaxation matrix Q are given by

$$A_{nm} = \frac{n+1}{2n+1}\,\delta_{n+1,m}\,, \qquad B_{nm} = \frac{n}{2n+1}\delta_{n-1,m}\,, \qquad Q_{nm} = \delta_{nm}(1 - \delta_{n,0})\,. \tag{30}$$

This system is linear hyperbolic. The eigenvalues of the matrix $A+B$ are the roots $\{\lambda_i\}_{i=1}^N \subset [-1, 1]$ of the polynomial p_{N+1}. In most applications, N is odd and these roots appear in pairs with opposite signs that accumulate at $\{\pm 1\}$ as $N \to \infty$. Corresponding to each eigenvalue λ_i is the right eigenvector $\mathbf{r}_i = \mathbf{p}(\lambda_i)$.

3.2 Leading Order Asymptotics and the Diffusion Limit

As one might expect, the P_N equations have the same diffusive limit as the transport equation (11). A simple way to see this limit is to introduce the moment vector $\bar{\mathbf{u}}$, whose components

$$\bar{u}_n := \varepsilon^{-n} u_n\,, \quad n = 0, \ldots, N\,, \tag{31}$$

are $O(1)$ quantities with respect to ε. (This follows from a simple asymptotic analysis of (29)). Note that $\bar{\phi} = \phi$. In terms of $\bar{\mathbf{u}}$, the P_N equations are

$$\partial_t \bar{\mathbf{u}} + \left(A + \frac{1}{\varepsilon^2} B\right) \partial_x \bar{\mathbf{u}} = -\frac{\sigma_s}{\varepsilon^2} Q\bar{\mathbf{u}} \tag{32}$$

and the expansion of ψ in (21) is

$$\psi(x, \mu, t) = \sum_{n=0}^{N} \frac{2n+1}{2} \varepsilon^n \bar{u}_n(x, t) p_n(\mu)\,. \tag{33}$$

While (14) follows immediately from (33), equation (15) is formally established by examining the first two equations in (32):

$$\partial_t \phi + \partial_x \bar{J} = 0\,, \tag{34a}$$

$$\partial_t \bar{J} + \frac{1}{\varepsilon^2}\frac{1}{3}\partial_x \phi + \frac{2}{3}\partial_x \bar{P} = -\frac{\sigma_s}{\varepsilon^2}\bar{J}\,. \tag{34b}$$

For ε small, (34b) implies that

$$\bar{J} = -\frac{1}{3\sigma_s}\partial_x\phi + O(\varepsilon^2) \tag{35}$$

which, upon substitution into (34a), recovers (15) in the limit $\varepsilon \to 0$.

More generally, the leading order balance for each component u_n, $n \geq 1$, can be easily determined from (31) and (32) and the formulas for B and Q in (30):

$$u_n = -\varepsilon\frac{n}{2n+1}\partial_x u_{n-1} = , \quad n \geq 1 . \tag{36}$$

For example, a recursive application of (36) gives

$$J = -\frac{1}{3}\varepsilon\partial_x\phi + O(\varepsilon^2) , \qquad P = \frac{2}{15}\varepsilon^2\partial_x^2\phi + O(\varepsilon^3) , \qquad q = -\frac{2}{35}\varepsilon^3\partial_x^3\phi + O(\varepsilon^4) . \tag{37}$$

3.3 Numerical Challenges: Stiffness and Excessive Numerical Dissipation

It is well known that conventional upwind methods for hyperbolic equations suffer from two major complications when applied to the P_N equations in diffusive regimes (For example, see [39].) These are (i) stiffness and (ii) excessive numerical dissipation. As an illustrative example of how upwind hyperbolic solvers fail, consider a scheme for the P_N equations that treats the hyperbolic part with the first-order upwind (Godunov) method and uses cell averages for the source terms. Such a scheme takes the following semi-discrete form:

$$d_t\mathbf{u}_j + \frac{1}{\varepsilon}M\frac{\mathbf{u}_{j+1} - \mathbf{u}_{j-1}}{2h} = -\frac{(\sigma_s)_j}{\varepsilon^2}Q\mathbf{u}_j + \frac{h}{\varepsilon}|M|\frac{\mathbf{u}_{j+1} - 2\mathbf{u}_j + \mathbf{u}_{j-1}}{2h^2} , \tag{38}$$

where $M = A + B$ (see (30)) and the second term on the right-hand side is the dissipation needed for stability near discontinuities. For ε small, the balance for the J equation in (38) is

$$J_j = -\varepsilon\left(\frac{1}{3(\sigma_s)_j}\frac{\phi_{j+1} - \phi_{j-1}}{2h} + O(h)\right) + O(\varepsilon^2) , \tag{39}$$

which, when substituted into the ψ equation in (38) gives

$$d_t\phi_j = \frac{1}{3}\frac{(\sigma_s)_{j+1}^{-1}(\phi_{j+2} - \phi_j) - (\sigma_s)_{j-1}^{-1}(\phi_j - \phi_{j-2})}{4h^2} + \frac{h}{\varepsilon}D_j^\phi + O(\varepsilon) + O(h) . \tag{40}$$

where D_j^ϕ is the first component of the $O(1)$ dissipation on the right-hand side of (38).[2] As $\varepsilon \to 0$, the first term on the right-hand side of (40) yields a consistent discretization of the diffusive flux on the right-hand side of (15). However, the second term on the right-hand side of (40)—the numerical dissipation term—will clearly affect the accuracy of the solution unless the mesh spacing h is chosen much smaller than ε—an expensive undertaking given that one need not resolve such small scales when discretizing the diffusion equation (15)

[2]For example, when $N = 1$, $D_j^\phi = \frac{1}{\sqrt{3}}\frac{\phi_{j+1} - 2\phi_j + \phi_{j-1}}{2h^2}$.

directly. The expense of resolving ε is exacerbated by a stiff hyperbolic CFL condition which requires that the time step τ in any temporal discretization of (38) satisfies

$$\tau < \varepsilon C h \tag{41}$$

for some $O(1)$ constant C. This restriction is onerous for very small ε, in some instances even compared with an explicit method for (15). Increasing the spatial order-of-accuracy will help decrease the dissipation. For example, for a Godunov-type scheme using a central-difference reconstruction, the numerical dissipation for smooth solutions improves to $O\left(h^3/\varepsilon\right)$ (see [39] for a specific case), but then very small ε is still problematic and the restrictive CFL condition in (41) does not improve.

3.4 Previous Work

A great deal of work to address excessive numerical dissipation has been done in the context of families of 2×2 systems, which include P_N for $N = 1$. Also known as the *hyperbolic heat equation*, the P_1 system is a relaxation model which, in terms of the variables ϕ and $\bar{J} = \varepsilon^{-1} J$, takes the form

$$\partial_t \phi + \partial_x \bar{J} = 0 \,, \tag{42a}$$

$$\partial_t \bar{J} + \frac{1}{3}\frac{1}{\varepsilon^2}\partial_x \phi = -\frac{\sigma_\mathrm{s}}{\varepsilon^2}\bar{J} \,. \tag{42b}$$

The mathematical aspects of this model and nonlinear variants have been studied both theoretically [37,30,45,40,41,49] and numerically [21,39,27]. Studies of relaxation in similar models can be found in the context of radiation and neutron transport [47, 35, 9, 22, 43] and also in drift-diffusion systems such as charge transport in semiconductors [24, 28, 50] and chemotaxis [17, 16].

Upon diagonalization, the P_1 system (42) takes the form of a Goldstein-Taylor model [19, 58] with wave speeds $\pm(3\varepsilon)^{-1/2}$. Indeed, if we set $\xi^\pm := \phi \pm \sqrt{3}\varepsilon\bar{J}$, then

$$\partial_t \xi^+ + \frac{1}{\varepsilon}\frac{1}{\sqrt{3}}\partial_x \xi^+ = -\frac{\sigma_\mathrm{s}}{2\varepsilon^2}(\xi^+ - \xi^-) \,, \tag{43a}$$

$$\partial_t \xi^- - \frac{1}{\varepsilon}\frac{1}{\sqrt{3}}\partial_x \xi^- = -\frac{\sigma_\mathrm{s}}{2\varepsilon^2}(\xi^- - \xi^+) \,. \tag{43b}$$

Meanwhile, the diffusive character of (42) is evident upon formally balancing powers of ε in (42b), that results in a closure for (42a) that is accurate up to $O(\varepsilon^2)$:

$$\bar{J} = -\frac{1}{3\sigma_\mathrm{s}}\partial_x \phi \,, \tag{44a}$$

$$\partial_t \phi = \partial_x \left(\frac{1}{3\sigma_\mathrm{s}}\partial_x \phi \right) \,. \tag{44b}$$

We briefly mention three approaches for solving (42). The first is an operator splitting approach [27, 26] which separates the fast and slow dynamics in (42). Following [55], this

method can be extended to the scaled transport equation (11) using an even-odd parity formulation. In particular, the even and (scaled) odd parts of ψ:

$$\psi^E(\mu) = \frac{1}{2}(\psi(\mu) + \psi(-\mu)) \,, \quad \psi^O(\mu) = \frac{1}{2\varepsilon}(\psi(\mu) - \psi(-\mu)) \,, \quad \mu \in [0,1] \,, \tag{45}$$

satisfy the 2×2 system

$$\partial_t \psi^E + \mu \partial_x \psi^O = -\frac{\sigma_\mathrm{s}}{\varepsilon^2}\left(\psi^E - \frac{1}{2}\phi\right) \,, \tag{46a}$$

$$\partial_t \psi^O + \frac{\mu}{\varepsilon^2}\partial_x \psi^E = -\frac{\sigma_\mathrm{s}}{\varepsilon^2}\psi^O \,, \tag{46b}$$

whose form (except for the harmless source term in (46a)) parallels that of (42).

A second approach [21] uses a well-balanced formalism based on steady-states solutions of (43). An extension to transport equations [22] uses another reformulation of the kinetic distribution in terms of positive and negative moving particles. In particular, the positive and negative moving components of ψ:

$$\psi^P(\mu) = \psi(\mu) \,, \quad \psi^N(\mu) = \psi(-\mu) \,, \quad \mu \in [0,1] \,, \tag{47}$$

satisfy the 2×2 system

$$\partial_t \psi^P + \frac{\mu}{\varepsilon}\partial_x \psi^P = -\frac{\sigma_\mathrm{s}}{\varepsilon^2}\left(\psi^P - \frac{1}{2}\phi\right) \,, \tag{48}$$

$$\partial_t \psi^N - \frac{\mu}{\varepsilon}\partial_x \psi^N = -\frac{\sigma_\mathrm{s}}{\varepsilon^2}\left(\psi^N - \frac{1}{2}\phi\right) \,, \tag{49}$$

which is a diagonalization of (46) whose form parallels that of (43).

A third approach is to use discontinuous Galerkin (DG) methods, which are based on a local expansion of the state variables in each cell[3]. Thus no reconstructions are required; instead the local expansion coefficients are evolved in time for each cell. Neighboring cells are coupled via the Riemann problem evaluated at cell boundaries, just as with many other high-resolution schemes. Nonphysical numerical oscillations must be suppressed, through either slope limiting, filtering, "flux fix-ups," or the addition of nonlinear dissipative terms. If the local expansion is simply a constant, then DG reduces to the first-order Godunov method, which does not have the diffusion limit (see Eq. (40)). But for transport and using a linear expansion, it is well known that DG will achieve the diffusion limit [31, 39].

In the following sections, we discuss recent and ongoing work for simulating general P_N systems. The first method [43] extends the DG approach from [39] to general N. The second method borrows ideas from [26] to derive modified equations for which the diffusion limit is built-in.

4 DG Methods

In this section we will apply the discontinuous Galerkin (DG) method [52, 33] to the P_N system. The DG method was first developed for linear transport [52]. Its asymptotic behavior

[3]Typically such an expansion is in space only, but expansions in both space and time are also used.

for steady solutions was first explored by Larsen and Morel [31] in the context of the discrete ordinates approximation. (This approximation can be interpreted in slab geometry as the P_N equations written in characteristic form, although the way in which the angular flux ψ is approximated is different.) Larsen and Morel used a linear basis and referred to the method as the linear discontinuous (LD) method. Our derivation will follow closely that of Larsen and Morel and is the neutron transport analog of that given in [43], which considered the case of thermal radiative transport.

4.1 Derivation

We begin the derivation by multiplying the P_N system (29) by a test function $\varphi \in C^\infty(\mathbb{R})$ and then integrating over the spatial cell I_j of length h to obtain the weak form:

$$\partial_t \int_{I_j} \varphi \mathbf{u}\, dx + \frac{1}{\varepsilon} M[\varphi \mathbf{u}]_j - \frac{1}{\varepsilon} M \int_{I_j} \mathbf{u}\, \partial_x \varphi\, dx = -\frac{1}{\varepsilon^2} Q \int_{I_j} \varphi \sigma_{\mathrm{s}} \mathbf{u}\, dx\,. \tag{50}$$

Here $M = A + B$ (see (30)), $[\cdot]_j \equiv (\cdot)_{j+1/2} - (\cdot)_{j-1/2}$, and the subscripts "$_{j+1/2,\ j-1/2}$" refer to the right and left boundaries of cell j, respectively. The unknown vector $\mathbf{u}(x,t)$ is approximated by an expansion of the form

$$\mathbf{u}(x,t) \approx \sum_{j=1}^{N_j} \sum_{\alpha=1}^{N_\alpha} \mathbf{u}_{\alpha,j}(t) b_\alpha(\xi_j(x))\,, \tag{51}$$

where N_j is the number of spatial cells in the domain and N_α is the number of basis functions. The basis functions $b_\alpha(\xi)$ are generally nonzero on the reference cell $\xi \in [0,1]$ but vanish outside this range. In the expansion (51), the mapping to the reference cell is given by

$$\xi_j(x) = \frac{1}{2} + \frac{1}{h}\left(x - x_j\right)\,, \tag{52}$$

where x_j is the cell center.

The Galerkin approach is to substitute (51) into (50) and then to set $\varphi(x) = \{b_\alpha(\xi_j(x))\}$ for each $\alpha = 1, \ldots, N_\alpha$ and each $j = 1, \ldots, N_j$. The resulting system of semidiscrete equations takes the form

$$\partial_t(\mathbf{W}\mathbf{U}_j) + \frac{M}{\varepsilon}\begin{pmatrix} -\mathbf{u}_{j-1/2} \\ \mathbf{u}_{j+1/2} \end{pmatrix} - \frac{1}{\varepsilon}\mathbf{K}\mathbf{V}_j = -\frac{(\sigma_{\mathrm{s}})_j}{\varepsilon^2}\mathbf{W}\mathbf{Q}_j\,, \tag{53}$$

where

$$\mathbf{U}_j = (\mathbf{u}_{1,j}, \mathbf{u}_{2,j}, \cdots, \mathbf{u}_{N\alpha,j})^T\,, \tag{54}$$

$$\mathbf{V}_j = (M\mathbf{u}_{1,j}, M\mathbf{u}_{2,j} \cdots, M\mathbf{u}_{N_\alpha,j})^T\,, \tag{55}$$

$$\mathbf{Q}_j = (Q\mathbf{u}_{1,j}, Q\mathbf{u}_{2,j} \cdots, Q\mathbf{u}_{N_\alpha,j})^T\,, \tag{56}$$

and the matrix elements of $\mathbf{W}$ and $\mathbf{K}$ are given by

$$W_{\alpha,\beta} = h\int_0^1 b_\alpha b_\beta\, d\xi\,, \qquad K_{\alpha,\beta} = \int_0^1 b_\alpha\left(\partial_\xi b_\beta\right) d\xi\,. \tag{57}$$

Also, as is standard practice in engineering codes, in (53) we assume that $\sigma_{\rm s}(x)$ varies slowly in each cell and approximate it as $(\sigma_{\rm s})_j := \sigma_{\rm s}(x_j)$.

A complete implementation of the semidiscrete system (50) requires specification of (i) a basis $\{b_\alpha(\xi)\}_{\alpha=1}^{N_\alpha}$; (ii) a time integrator; (iii) a Riemann solver to evaluate fluxes at cell edges (where the representation (51) may be discontinuous); and (iv) a method to suppress numerical oscillations.

4.2 Implementation Details

4.2.1 Linear Basis Functions

We now specialize the above derivation for a linear basis, given by

$$b_1(\xi) = 1 - \xi\,, \qquad b_2(\xi) = \xi\,. \tag{58}$$

With this choice, (58) gives that $\mathbf{u}_{1,j}(t)$ is the value on the left side of the cell ($\xi = 0$), while $\mathbf{u}_{2,j}(t)$ is the value on the right side ($\xi = 1$). This expansion is discontinuous in the sense that in general $\mathbf{u}_{2,j} \neq \mathbf{u}_{1,j+1}$ even though those two values are located at the same point in physical space. We also have that

$$\mathbf{W} = \frac{h}{6}\begin{pmatrix} 2 & 1 \\ 1 & 2 \end{pmatrix}, \qquad \mathbf{K} = \frac{1}{2}\begin{pmatrix} -1 & -1 \\ 1 & 1 \end{pmatrix}. \tag{59}$$

4.2.2 Time Integration

As in [43], the time integration is carried out using a simple predictor-corrector method, defined by the following steps:

1. Predictor:

$$\mathbf{W}\frac{\mathbf{U}_j^{k+1/2} - \mathbf{U}_j^k}{\Delta t/2} + \frac{1}{\varepsilon}\begin{pmatrix} -(M\mathbf{u})_{j-1/2} \\ (M\mathbf{u})_{j+1/2} \end{pmatrix}^k - \frac{1}{\varepsilon}\mathbf{K}\mathbf{V}_j^k = -\frac{(\sigma_{\rm s})_j}{\varepsilon^2}\mathbf{W}\mathbf{Q}_j^{k+1/2}\,, \tag{60a}$$

2. Corrector:

$$\mathbf{W}\frac{\mathbf{U}_j^{k+1} - \mathbf{U}_j^k}{\Delta t} + \frac{1}{\varepsilon}\begin{pmatrix} -(M\mathbf{u})_{j-1/2} \\ (M\mathbf{u})_{j+1/2} \end{pmatrix}^{k+1/2} - \frac{1}{\varepsilon}\mathbf{K}\mathbf{V}_j^{k+1/2} = -\frac{(\sigma_{\rm s})_j}{\varepsilon^2}\mathbf{W}\mathbf{Q}_j^{k+1}\,. \tag{60b}$$

where the superscript-k denotes the time level and Δt is the time step. In the limit $(\sigma_{\rm s})_j \to 0$, this time integration method reduces to second-order Runge-Kutta, which is commonly used with DG for hyperbolic conservation laws [14].

4.2.3 Evaluation of Boundary Fluxes

The cell-boundary fluxes $M\mathbf{u}_{j\pm1/2}$ are defined via the upwind flux

$$M\mathbf{u}_{j+1/2} = M\bar{\mathbf{u}}_{j+1/2} - \frac{1}{2}|M|\Delta\mathbf{u}_{j+1/2}\,. \tag{61}$$

Here $|M| = R|\Lambda|R^{-1}$, where $M = R\Lambda R^{-1}$ is the standard eigendecomposition of M, and

$$\bar{\mathbf{u}}_{j+1/2} = \frac{1}{2}(\mathbf{u}_{2,j} + \mathbf{u}_{1,j+1})\,, \qquad \Delta\mathbf{u}_{j+1/2} = \mathbf{u}_{1,j+1} - \mathbf{u}_{2,j}\,. \tag{62}$$

4.2.4 Slope Limiting

It is well known that a linear, second-order method for hyperbolic equations (such as DG with linear elements) will produce artificial oscillations in the solution; this is a result of Godunov's theorem. (See, for example, [34].) Therefore, we use a slope limiter to guarantee a non-oscillatory solution [14]. Other techniques have been used in the transport community to address oscillatory behavior. Mass matrix lumping [2] approximates $\mathbf{W}$ as a diagonal matrix, which effectively adds dissipation to damp oscillations; the oscillations are not fully eliminated because the method remains linear and second-order accurate. Also, engineering neutron codes sometimes use what is colloquially referred to as "flux fix-ups" [56, 42]. This "fix" sets any negative value of ϕ to zero, which is nonconservative and does not suppress numerical oscillations that may occur away from zero values.

Following Ref. [14], we invoke the slope limiter after each step in the time-integration (whether predictor or corrector). We first compute the average in each cell:

$$\bar{\mathbf{u}}_j = \frac{1}{2}\left(\mathbf{u}_{1,j} + \mathbf{u}_{2,j}\right) , \tag{63}$$

and then set the node values in the cell as

$$\tilde{\mathbf{u}}_{1,j} = \bar{\mathbf{u}}_j - \frac{\mathbf{s}_j}{2} \quad \text{and} \quad \tilde{\mathbf{u}}_{2,j} = \bar{\mathbf{u}}_j + \frac{\mathbf{s}_j}{2} ,$$

where the slope

$$\mathbf{s}_j = \text{minmod}(\mathbf{u}_{2,j} - \mathbf{u}_{1,j}, \theta(\bar{\mathbf{u}}_j - \bar{\mathbf{u}}_{j-1}), \theta(\bar{\mathbf{u}}_{j+1} - \bar{\mathbf{u}}_j)), \tag{64}$$

is computed component-wise and $\theta \in [0, 2]$. Choosing $\theta = 0$ results in the first-order upwind, or Godunov, scheme. In the transport literature, this method is also known as the "step" scheme. The step scheme is known to be inaccurate in the diffusion limit [32] (see also Eq. (40)) and will not be considered further here. With $\theta = 1$ the limiter is identical to the minmod limiter [34]. Recently, it has been shown that the minmod limiter can cause the DG method to fail to be asymptotic preserving [44]. When $\theta = 2$ we have the monotonized center or double minmod limiter [59]. The double minmod limiter is robust in the diffusion limit, though it can create "sawtoothing" at cell edges [44], in that although the cell averages are monotone, the linear representation (51) may create local extrema at a cell edge. For most of the computations presented here, we use $\theta = 2$ for the remainder of our study. The only exceptions are the computational results that are presented in Figures 3 and 4. For these calculations, the solution is smooth and no limiter is used. The issue here is that higher order moments become spatial gradients of lower order moments in the diffusion limit. Thus clipping by slope limiters can create numerical artifacts and must be implemented with care.
—-

4.3 Properties

The DG method with semi-implicit time integration and linear basis functions has the following properties:

1. **Asymptotic Preservation.** As $\varepsilon \to 0$, the method outlined above reduces to a robust discretization of the diffusion equation (14). In this limit, the DG method transitions to a continuous finite element discretization [31]. Specifically, $\mathbf{u}_{2,j} = \mathbf{u}_{1,j+1} \equiv \mathbf{u}_{j+1/2}$ and the flux J reduces to

$$J_{i,j}^{k+1} = -\frac{\varepsilon}{3(\sigma_\mathrm{s})_j} \frac{\phi_{j+1/2}^k - \phi_{j-1/2}^k}{h} \,, \tag{65}$$

which is a discrete form of (35). Moreover, ϕ is governed by

$$\frac{1}{6} \frac{\breve{\phi}_j^{k+1} - \breve{\phi}_j^k}{\Delta t} = \frac{1}{3\sigma_\mathrm{s}} \frac{\phi_{j+3/2}^k - 2\phi_{j+1/2}^k + \phi_{j-1/2}^k}{2h^2} \,, \tag{66}$$

where

$$\breve{\phi}_j = \phi_{j+3/2} + \phi_{j+1/2} + \phi_{j-1/2} \,, \tag{67}$$

and for simplicity we have assumed a constant value for σ_s. Equation (66) is the continuous, piecewise linear finite-element discretization of (14) integrated with the forward-Euler method.

If the advection term in (53) is integrated using forward-Euler time integration rather than second-order Runge-Kutta, then the corresponding asymptotic discretization would be "doubly-lagged;" that is, the terms on the right-hand side of (66) are then evaluated at the $k-1$ time level [29]. Such a time integration scheme is less accurate than (66) and requires smaller time steps for stability. More importantly, forward Euler for (53) is unconditionally unstable in the limit $\sigma_\mathrm{s} \to 0$.

2. **Local Implicitness.** In the above time integration scheme the scattering operator is treated in a locally implicit manner. That is, the implicit terms couple only values within a mesh cell and are decoupled from neighboring cells.

3. **Time Step Restriction.** The advantage of local implicitness comes at a cost. The time integration method treats the advection terms using second-order Runge-Kutta integration and the scattering operator using two backward Euler steps; in this sense the time integration method is semi-implicit. Due to the explicit treatment of the advection terms, the predictor-corrector time integration method has a CFL limit of $\Delta t \leq \varepsilon h/3$ [14].

Unfortunately, the time step restriction of our DG implementation follows that given by (41), even in the diffusion limit. This restriction is typically overcome by using implicit time integration. But in the next section, we consider a finite-volume method that overcomes this time step restriction in the diffusion limit.

5 Temporal Regularization

Temporal regularization is an approach for simulating the P_N equations that is based on a separation of dynamics into fast and slow time scales. Regularized equations are derived using an operator splitting techniques first derived in [26] for 2×2 systems with constant cross-sections. Very recently, the approach has been extended in [25] to linear, one-dimensional systems.

5.1 Derivation

Regularized equations are derived by splitting the original P_N system (29) into a relaxation step and a convection step as follows:

1. Relaxation:
$$\partial_t \mathbf{u} + \frac{1}{\varepsilon} B \partial_x \mathbf{u} = -\frac{1}{\varepsilon^2} Q \mathbf{u} \,, \tag{68a}$$

2. Convection:
$$\partial_t \mathbf{u} + \frac{1}{\varepsilon} A \partial_x \mathbf{u} = 0 \,. \tag{68b}$$

This splitting was introduced in [25] and is motivated by the balance of terms in (32) in terms of the rescaled components of $\bar{\mathbf{u}}$. In the relaxation step, source terms are updated implicitly, and flux terms explicitly. This gives an intermediate value for $\mathbf{u}$:

$$\mathbf{u}^{k+1/2} = \Gamma \mathbf{u}^k + \frac{\Delta t}{\varepsilon} \Gamma B \partial_x \mathbf{u}^k \,, \tag{69}$$

where Δt is the computational time step and Γ is a diagonal matrix with components

$$\Gamma_{11} = 1 \qquad \text{and} \qquad \Gamma_{nn} = \gamma := \frac{\varepsilon^2}{\varepsilon^2 + \sigma_{\mathrm{s}} \Delta t} \,, \quad n > 1 \,. \tag{70}$$

Applying the convection step (68b) with initial condition $\mathbf{u}^{k+1/2}$ gives

$$\begin{aligned} \mathbf{u}^{k+1} &= \mathbf{u}^{k+1/2} - \frac{\Delta t}{\varepsilon} A \partial_x \mathbf{u}^{k+1/2} \\ &= \Gamma \mathbf{u}^k - \frac{\Delta t}{\varepsilon} \left(A \partial_x (\gamma \mathbf{u}^k) + \gamma B \partial_x \mathbf{u}^k \right) + \frac{\Delta t^2}{\varepsilon^2} AB (\gamma \partial_x \mathbf{u}) \,. \end{aligned} \tag{71}$$

Here we have used the fact that, due to the special form of A and B (see (30)),

$$A\Gamma = \gamma A \qquad \text{and} \qquad \Gamma B = \gamma B \,. \tag{72}$$

The temporal discretization (71) is an $O(\Delta t)$ approximation of the following *regularized* P_N (or RP_N) system

$$\partial_t \mathbf{u} + \frac{1}{\varepsilon} \left(A \partial_x (\gamma \mathbf{u}) + \gamma B \partial_x \mathbf{u} \right) = -\frac{\gamma \sigma_{\mathrm{s}}}{\varepsilon^2} Q \mathbf{u} + \frac{\Delta t}{\varepsilon^2} AB \partial_x (\gamma \partial_x \mathbf{u}) \,, \tag{73}$$

which is derived by letting $\Delta t \to 0$ in (71) *only in evaluating the time derivative* of $\mathbf{u}$.

5.2 Properties

The regularized P_N system (73) has the following properties:

1. **Increased Time Step.** The local wave speeds of (73) are of the order

$$\frac{\gamma}{\varepsilon} = \frac{\varepsilon}{\varepsilon^2 + \sigma_{\mathrm{s}}\Delta t} \,. \tag{74}$$

Thus we can enforce a global stability conditions by setting

$$\frac{\varepsilon}{\varepsilon^2 + \sigma_{\mathrm{s}}\Delta t}\Delta t < Ch \,, \tag{75}$$

where C is an $O(1)$ constant that depends on the particular choice of a numerical scheme. There are two cases:

   (a) When ε is resolved by the mesh spacing ($\varepsilon > Ch\sigma_{\mathrm{s}}$), the worst-case restriction on the time step occurs when $\varepsilon = 2C\sigma_{\mathrm{s}}h$. In this case, (75) gives a time step consistent with an explicit diffusion scheme:

$$\Delta t < 4C^2\sigma_{\mathrm{s}}h^2 \,. \tag{76}$$

   A similar time step is required by schemes found in [21, 27] for the P_1 system in the diffusive limit.

   (b) When ε is *under-resolved* ($\varepsilon < Ch/\sigma_{\mathrm{s}}$), there is no hyperbolic time step restriction induced by (75). In such cases, an implicit discretization of the diffusion terms in (73) leads to scheme for which the time step restriction is based entirely on accuracy considerations. This is one of the more powerful features of the method from an applications point of view since, in many cases, an explicit diffusion condition—while better than (41)—is still too restrictive. Moreover, because the matrix AB is diagonal, solving the diffusion terms implicitly is relatively simple.

2. **Asymptotic Accuracy.** When $\Delta t \sim h^2 \sim \varepsilon^2$ and $\sigma_{\mathrm{s}} = O(1)$ is constant, the wave speeds of (73) are $O(h^{-1})$:

$$|\lambda_{\pm}| \sim \frac{1}{h} \,. \tag{77}$$

In such cases, the numerical dissipation in a first order upwind scheme for (73) will be $O(1)$. Therefore higher-order schemes (such as the MUSCL-type scheme used in [26]) are required to ensure that the discretization of (73) is AP in all regimes. One must still accept a loss of spatial accuracy, but such losses are limited to one drop in order: In general, the worst-case dissipation for a standard Godunov-type method with $O(h^r)$ spatial reconstructions will be $O(h^{r-1})$. For non-constant cross-sections, the situation can be more delicate, as discussed in the next section.

3. **The Diffusion Limit.** For $\sigma_{\mathrm{s}}\Delta t$ fixed and positive,

$$\lim_{\varepsilon\to 0}\gamma = 0 \quad \text{and} \quad \lim_{\varepsilon\to 0}\frac{\gamma}{\varepsilon^2} = \frac{1}{\sigma_{\mathrm{s}}\Delta t} \,. \tag{78}$$

Hence the equation for ρ in (73):

$$\partial_t\rho + \partial_x(\gamma m) = \frac{\Delta t}{3\varepsilon^2}\partial_x(\gamma\partial_x\rho) \,, \tag{79}$$

formally recovers the diffusion equation (44) the limit as $\varepsilon \to 0$.

4. **Balance for Higher Moments.** For $\sigma_s \Delta t$ fixed and positive, J has the correct leading order balance up to an $O(\Delta t)$ correction. Furthermore, although the numerical balance for higher order moments ($n > 1$) is not consistent with (36) after a single time step, it will be (up to an $O(\Delta t)$ error) after a finite number of time steps [25].

5.3 Implementation Details

5.3.1 Constant Cross-section

When σ_s is constant, a simple numerical scheme for (73) is constructed using an explicit, conservative discretization of the convective terms and the canonical implicit discretization of the diffusive terms. In vector notation, the scheme takes the form

$$\mathbf{u}_j^{k+1} = \Gamma \mathbf{u}_j^k - \frac{\Delta t}{\varepsilon} M_\gamma \frac{\mathbf{u}_{j+1/2}^k - \mathbf{u}_{j-1/2}^k}{h} + \frac{\Delta t^2 \gamma}{\varepsilon^2} AB \frac{\mathbf{u}_{j+1}^{k+1} - 2\mathbf{u}_j^{k+1} + \mathbf{u}_{j-1}^{k+1}}{h^2}, \tag{80}$$

where $M_\gamma := \gamma(A+B)$ and $\mathbf{u}_j^k$ is the average of $\mathbf{u}$ at time $t_k := k\Delta t$ over a cell I_j with width h.

The edge fluxes $M_\gamma \mathbf{u}_{j\pm1/2}^k$ in (80) are determined using a second-order upwind method:

$$M_\gamma \mathbf{u}_{j+1/2}^k = \frac{1}{2} M_\gamma \left(\mathbf{u}_{j+1/2}^{k,l} + \mathbf{u}_{j+1/2}^{k,r} \right) + \frac{1}{2} |M_\gamma| \left(\mathbf{u}_{j+1/2}^{k,l} - \mathbf{u}_{j+1/2}^{k,r} \right), \tag{81}$$

where the matrix $|M_\gamma| := R_\gamma |\Lambda_\gamma| R_\gamma^{-1}$ is calculated using the eigenvectors and eigenvalues from the diagonalization $M_\gamma = R_\gamma \Lambda_\gamma R_\gamma^{-1}$ of the matrix M_γ. The right and left edge values of $\mathbf{u}$ in (81) are given by

$$\mathbf{u}_{j+1/2}^{k,l} = R_\gamma \mathbf{w}_{j+1/2}^{k,l} \qquad \text{and} \qquad \mathbf{u}_{j+1/2}^{k,r} = R_\gamma \mathbf{w}_{j+1/2}^{k,r}, \tag{82}$$

and the characteristic edge values are determined by linear reconstructions on adjacent cells:

$$\mathbf{w}_{j+1/2}^{k,l} = \mathbf{w}_j^k + \frac{h}{2} \mathbf{w}_j' \qquad \text{and} \qquad \mathbf{w}_{j+1/2}^{k,r} = \mathbf{w}_{j+1}^k - \frac{h}{2} \mathbf{w}_{j+1}', \tag{83}$$

where $\mathbf{w}_j^k := R_\gamma^{-1} \mathbf{u}_j^k$ and the slopes $\mathbf{w}_j'$ approximate derivatives in each cell. For $O(1)$ or greater values of ε, we set $\mathbf{w}_j'$ with a minmod-type limiter:

$$\mathbf{w}_j' = \frac{1}{h} \operatorname{minmod} \left(\theta(\mathbf{w}_{j+1} - \mathbf{w}_j), \frac{1}{2}(\mathbf{w}_{j+1} - \mathbf{w}_{j-1}), \theta(\mathbf{w}_j - \mathbf{w}_{j-1}) \right) \tag{84}$$

that is applied component-wise with $\theta = 2$. However, in diffusive regimes, we have observed small glitches near extrema of the higher order moments beyond ϕ and J that is due to clipping. These glitches vanish under mesh refinement and appear only in higher order moments. Other limiters—including (84) with $\theta = 1$, the Van Leer limiter, and the superbee limiter—produce similar effects. Similar to the DG method, we currently use a linear reconstruction with no limiter in diffusive regimes, where the solution is presumably smooth, in order to avoid numerical artifacts for the higher order moments beyond ϕ and J. An in-depth analysis of limiter effects is ongoing.

5.3.2 Spatially Varying Cross-section

When $\sigma_{\rm s}$ is not constant in space, discretizing (73) is more challenging because of the presence of non-conservative convection terms. We utilize the wave-splitting technique from [5] that was developed to solve hyperbolic systems with spatially varying fluxes. The wave-splitting method can also be applied to systems with source terms, which are directly incorporated into the algorithm's Riemann solver. The idea of balancing fluxes and source terms in this way has been advocated in [53] in the context of Euler equations and also in [54] in a more general context. The general notion of upwinding source terms has also been a basic building block for the numerical schemes found in [17, 4, 7].

To use the wave-splitting technique, we first apply Leibniz rule to the term $\gamma B\partial_x(\mathbf{u}^k)$ and rewrite (73) in conservation form:

$$\partial_t \mathbf{u} + \frac{1}{\varepsilon}(A+B)\partial_x(\gamma\mathbf{u}) = -\frac{\gamma\sigma_{\rm s}}{\varepsilon^2}Q\mathbf{u} + \frac{\Delta t}{\varepsilon^2}AB\partial_x\left(\gamma\partial_x\mathbf{u}\right) + \frac{1}{\varepsilon}B(\partial_x\gamma)\mathbf{u}\,. \tag{85}$$

This reformulation ensures that the discretization of (79) will be conservative. The trade-off is that we must properly interpret the term $B(\partial_x\gamma)\mathbf{u}$, even when the cross-section is discontinuous in space.

As before, we let $\mathbf{u}_j^k$ be the average of $\mathbf{u}$ at time $t_k = k\Delta t$ over a cell I_j of width h. Following the recipe in [5] (but with different notation), we introduce, at each cell interface, the quantity

$$\mathbf{\Delta}_{j+1/2}^k := \frac{1}{\varepsilon}(A+B)(\gamma_{j+1}\mathbf{u}_{j+1}^k - \gamma_j\mathbf{u}_j^k) + \frac{\gamma\sigma_{\rm s}}{\varepsilon^2}Q\mathbf{u}_j^k - \frac{1}{2\varepsilon}B(\gamma_{j+1}-\gamma_j)(\mathbf{u}_{j+1}^k + \mathbf{u}_j^k)\,, \tag{86}$$

which is a first order (in space) approximation of the jump across the interface due to flux differences, the source term $\varepsilon^{-2}\gamma\sigma_{\rm s}Q\mathbf{u}_j^k$, and the nonconservative term $\varepsilon^{-1}B(\partial_x\gamma)\mathbf{u}$. We then update $\mathbf{u}$ as follows:

$$\begin{aligned}\mathbf{u}_j^{k+1} = \mathbf{u}_j^k &- \frac{\Delta t}{h}\left(R_\gamma^- L_\gamma^- \mathbf{\Delta}_{j+1/2}^k + R_\gamma^+ L_\gamma^+ \mathbf{\Delta}_{j-1/2}^k\right) \\ &+ \frac{\Delta t^2}{\varepsilon^2 h}AB\left((\gamma\partial_x\mathbf{u})_{j+1/2}^{k+1} - (\gamma\partial_x\mathbf{u})_{j-1/2}^{k+1}\right)\,.\end{aligned} \tag{87}$$

Here $R_\gamma^\pm$ and $L_\gamma^\pm$ are matrices of size $(N+1)\times(N+1)/2$ and $(N+1)/2\times(N+1)$, respectively, which contain the left and right eigenvectors corresponding to positive and negative eigenvalues of the matrix $\gamma(A+B)$. By an appropriate choice of scaling, these matrices can be chosen are independent of γ—hence constant in space and computed only once. The diffusive fluxes in (87) are given by

$$(\gamma\partial_x\mathbf{u})_{j+1/2} = \gamma_{j+1/2}\frac{\mathbf{u}_{j+1}-\mathbf{u}_j}{h}\,, \tag{88}$$

where $(\Delta t\gamma)_{j+1/2}$ is the harmonic average of cell values to the right and left of the interface.

A second order version of the wave-splitting scheme is designed in [5] by adding flux and source term corrections derived from a Taylor expansion analysis. Since the regularization

is only an $O(\Delta t)$ accurate approximation of the original P_N system we only include flux corrections to improve spatial accuracy:

$$\begin{aligned}\mathbf{u}^{k+1} = \mathbf{u}^k &- \frac{\Delta t}{h}\left(R_\gamma^- L_\gamma^- \mathbf{\Delta}_{j+1/2}^k + R_\gamma^+ L_\gamma^+ \mathbf{\Delta}_{j-1/2}^k\right) \\ &- \frac{\Delta t}{h}\left(\tilde{F}_{j+1/2} - \tilde{F}_{j-1/2}\right) + \frac{\Delta t^2}{\varepsilon^2 h} AB\left((\gamma \partial_x \mathbf{u})_{j+1/2}^{k+1} - (\gamma \partial_x \mathbf{u})_{j-1/2}^{k+1}\right), \end{aligned} \tag{89}$$

where, following [5], the flux corrections are given by

$$\tilde{F}_{j+1/2} = \frac{1}{2}\sum_{n=0}^{N} \operatorname{sgn}(\lambda_{j+1/2}^n)\left(1 - \frac{\Delta t}{\varepsilon h}|\lambda_{j+1/2}^n|\right)\mathcal{L}\left\{\mathbf{r}^n (\mathbf{l}^n)^T \mathbf{\Delta}_{j+1/2}^k\right\}. \tag{90}$$

Here $\{\lambda_{j+1/2}^n\}_{n=0}^N$ are the eigenvalues of the matrix $\gamma(A+B)$, evaluated on the upwind side of the cell interface, and the vectors $\{\mathbf{r}^n\}_{n=0}^N$ and $\{\mathbf{l}^n\}_{n=0}^N$ are the right and left eigenvectors of this matrix (which do not vary in space). The operator $\mathcal{L}$ is a limiter given by

$$\mathcal{L}(\mathbf{q}_{j+1/2}) := \phi\left(\frac{|\mathbf{q}_{j+1/2}|}{|\mathbf{q}_{j'+1/2}|}\right)\mathbf{q}_{j+1/2} \tag{91}$$

for some choice of smoothness indicator ϕ, where the notation $|\cdot|$ denotes the standard Euclidian norm and j' is the index on the upwind side of the interface $x_{j+1/2}$. Note that without the source term, (89) is just a limited Lax-Wendroff scheme for the left-hand side of (85).

Unfortunately, the addition of flux corrections to our scheme is not always stable. In streaming regimes, the only limiter that is consistently stable is the minmod limiter $\phi(\theta) = \text{minmod}(1, \theta)$. Worse yet, in diffusive regimes, there are cases when our implementation of (89) is unstable for the minmod limiter as well, even when the cross-section varies smoothly. Numerical experiments show that the onset of instability is marked by negative values for the scalar flux ϕ which, by definition, is a non-negative quantity. It is almost certain that the source of this instability is the naïve treatment of the non-conservative term on the right-hand side of (85), and further analysis is clearly needed here. Even so, the results of the next section clearly indicate the potential of the regularization method.

6 Numerical Tests

In this section, we present preliminary results for the DG and regularization approaches on a series of simple test problems. The problems are divided into three groups according to the profile of the cross-section $\sigma_s(x)$:

1. Constant (non-zero) cross-section.
2. Vanishing cross-section, in that $\sigma_s(x)$ is zero somewhere in the domain.
3. Discontinuous cross-section.

The goal of these tests is to show that the DG and regularization methods produce numerically accurate results in a variety of test cases, but at a resolution that is comparable to or less than that of a conventional upwind scheme. This benefit will become more apparent as ε becomes small relative to the spatial mesh, as is common in the diffusion limit.

All test problems are defined on the interval $x \in [0, 2]$, with periodic boundary conditions and the initial condition

$$\phi(x, 0) = \begin{cases} 2.0, & x \in (0.8, 1.2) \ , \\ 0.0, & x \in [0.0, 0.8] \cup [1.2, 2.0] \ . \end{cases} \tag{92}$$

All other moments are set initially to zero.

Constant Cross-section. In our first test, we consider a constant cross-section $\sigma_{\rm s} = 1$. By selecting $N = 3$, we can conveniently display results for all four moments. For comparison, we include a standard upwind algorithm for (29) that is first order in time—updating fluxes explicitly and source terms implicitly—and second order in space. It takes the form

$$\mathbf{u}_j^{k+1} = \mathbf{u}_j^k - \frac{\Delta t}{\varepsilon} M \frac{\mathbf{u}_{j+1/2}^k - \mathbf{u}_{j-1/2}^k}{h} - \frac{\Delta t (\sigma_{\rm s})_j}{\varepsilon^2} \mathbf{u}_j^{k+1} \ , \tag{93}$$

where $\mathbf{u}_j^k$ is the average of $\mathbf{u}$ at time $t_k = k\Delta t$ over a cell I_j of width h and the approximation of fluxes at cell edges follows the same recipe that was prescribed for the regularized system in equations (81)-(84). In particular, (93) uses the second-order upwind method from (81) (with $\gamma = 1.0$) along with linear reconstructions based on characteristic variables (as in (83)) to approximate the edges fluxes $M\mathbf{u}_{j\pm1/2}^k$. For the case $\varepsilon = 2.0$ (see Figure 1 below), slope limiting is implemented using the limiter given by (84) with $\theta = 2.0$.

Results for $\varepsilon = 2.0$ are presented in Figure 1 at low-resolution (100 cells) and in Figure 2 at high-resolution (1000 cells). All results plot only the cell averages. For both meshes, the three algorithms give comparable results with comparable resolution, and it is clear that the all three methods are converging. The discontinuities in the DG scheme are a bit sharper, but one should keep in mind that DG uses twice the degrees-of-freedom as the finite-volume method. The DG results also show small overshoots near local extrema, possibly a result of limiting the moment variables instead of the characteristic variables.

The real benefit of the DG and regularization methods is realized when ε is very small. Indeed, as ε continues to get smaller, the upwind scheme requires addition resolution to maintain accuracy while DG and the regularization do not. Figure 3 shows results for each method with low resolution (100 cells) and $\varepsilon = 10^{-4}$. Here, both DG and the regularization method properly capture the diffusion limit for ϕ , while the standard upwind scheme does not. (Note that, although the cell-average values for DG are smooth, the linear representation of the moments other than ϕ display a sawtooth behavior in diffusion regimes.) Increasing the resolution of the upwind scheme to by a factor of ten does yield in an accurate solution of ϕ (see Figure 3). At the higher resolution, the upwind simulation of higher order moments (see (37)) is still inaccurate, although, in practice, these discrepancies become less important as ε becomes small because magnitude of these becomes very small. It should also be noted that the DG results for q are also inaccurate.

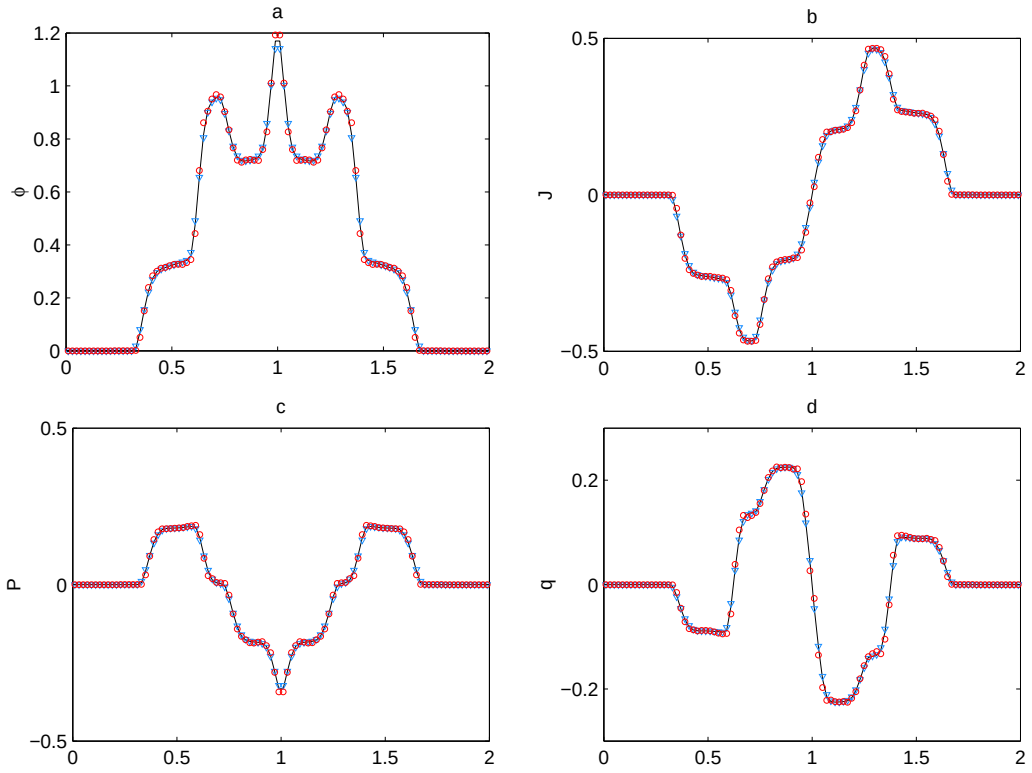

Figure 1: Constant cross-section, low resolution ($h = 0.02$) results, with $N = 3$, $\varepsilon = 2.0$, and at $t = 1.0$. Solid line: the upwind scheme with $\Delta t = 0.1h$; circles: DG with $\Delta t = 0.3\varepsilon h$; triangles: regularization with $\Delta t = 0.1h$.

By lowering ε even further, we see in Figure 5 that the 100-cell, upwind solution is essentially flat while the 1000 point solution has lost accuracy—particularly near its peak—when compared to the $\varepsilon = 10^{-4}$ case. In contrast, the DG and regularization methods continue to predict the correct diffusion limit with only 100 spatial cells. However, it should be noted that for values of ε this small, the regularization simulation is much more efficient. In particular, while the DG time step scales with ε, the regularization time step is based solely on accuracy requirements. (For the computations in Figure 5, the regularization time step is $\Delta t = 0.1h$.)

6.1 Vanishing Cross-section.

For this test, we set $\varepsilon = 10^{-3}$, $N = 7$, and consider the smoothly varying cross-section

$$\sigma_s(x) = 100(x-1)^4\,, \tag{94}$$

which is large at the edges of the domain but vanishes in the center. The vanishing cross-section means that, even though ε is relatively small, the scaled P_N system is essentially a wave equation with $O(1/\varepsilon)$ wave speeds near $x = 1$.

The vanishing cross-section (94) has also been considered in [9] for a nonlinear version of the P_1 system . In that work, a fully implicit scheme was used in order to overcome

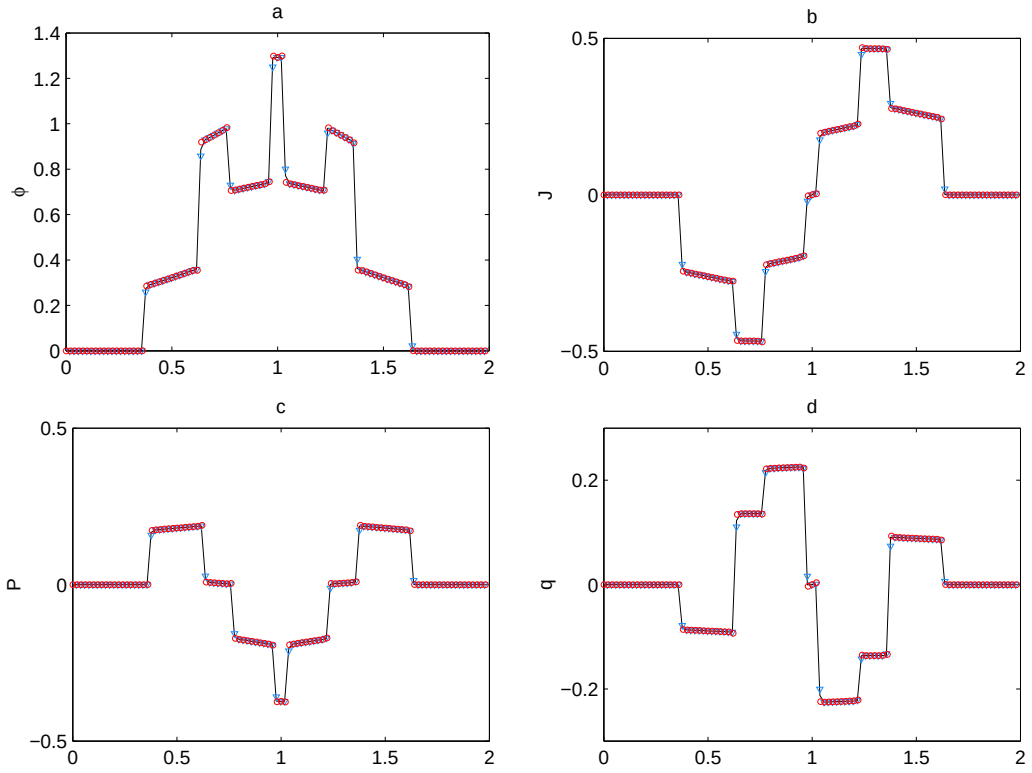

Figure 2: Same case as Fig. 1, but with high resolution ($h = 0.002$). Solid line: the upwind scheme with $\Delta t = 0.1h$; circles: DG with $\Delta t = 0.3\varepsilon h$; triangles: regularization with $\Delta t = 0.1h$.

the fast wave speeds in the center of the domain. In some applications, this approach may be preferred. However, one must be willing to sacrifice resolution of the hyperbolic wave structures in order to take time steps beyond the hyperbolic CFL condition.

As discussed in [25], the vanishing cross-section presents difficulties for Godunov-type discretizations of the RP_N system (73) which, at $x = 1$, is identical to the original P_N system (because $\gamma = 1$ there). For *global* stability, the CFL condition (75) must be satisfied for all values of σ_s. In particular, enforcing (75) in the center of the domain—where $\sigma_s = 0$ and the dynamics are *not* diffusive—requires that $\Delta t \leq Ch\varepsilon$. This small time step does not provide enough of a regularizing effect in regions of the domain where there the dynamics are diffusive, particularly in cases where $h = O(\varepsilon)$. In such situations, it is the wave-splitting algorithm that maintains the asymptotic preserving property by including source terms in the Riemann solver (see [25, Proposition 2]).

In Figure 6, profiles for ϕ for the vanishing cross-section test are presented for both the DG and regularization methods using only 25 computational cells. For comparison, results for the upwind scheme are given for 25, 50, and 100 cells. An 'exact' solution using the upwind scheme with 1000 cells is provided as a reference. As with the constant cross-section, these results show that the upwind method requires higher resolution than either the DG or regularized methods in order to obtain accurate solutions.

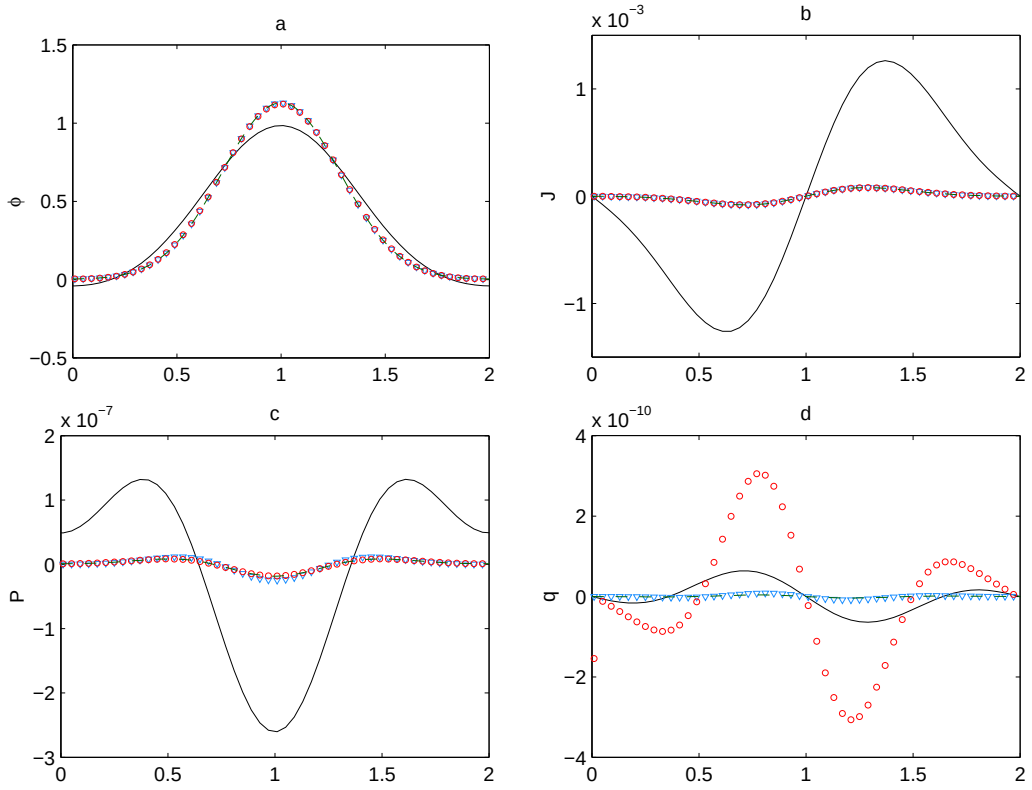

Figure 3: Same case as Fig. 1 (low resolution, $h = 0.02$), but with $\varepsilon = 10^{-4}$ and at time $t = 0.1$. Solid line: the upwind scheme with $\Delta t = 0.1\varepsilon h$; circles: DG with $\Delta t = 0.3\varepsilon h$; triangles: regularization with $\Delta t = 0.1h$. The diffusion solution (dashed line) is also plotted but not easily visible due to overlap.

6.2 Discontinuous Cross-section.

In our final test, we again let $N = 7$, but now consider a discontinuous cross-section

$$\sigma_s(x) = \begin{cases} 0.02, & x \in [0.35, 0.65] \cup [1.35 \cup 1.65]\,, \\ 1.0, & x \in [0, 0.35) \cup (0.65, 1.35) \cup (1.65, 2]\,. \end{cases} \tag{95}$$

We compute solutions using the DG scheme and the regularization method for three different regimes: (i) a kinetic regime ($\varepsilon = 2.0$), (ii) a transition regime ($\varepsilon = 4.0 \times 10^{-2}$), and (iii) a diffusive regime ($\varepsilon = 10^{-5}$). Results of these calculations for the scalar flux ϕ and the current J are shown in Figure (7).

In the kinetic regime (Figures 7a-b), the regularized equations are solved using a wave-splitting algorithm with flux corrections. The results are slightly more dissipative than for the DG solver, which uses the limiter in (84) with $\theta = 2$ and the two-step time integrator (60a)-(60b). As discussed in the last paragraph of Section 5, our current implementation of the wave-splitting with flux corrections (89) is not always stable. We therefore use the limiter (91) with $\theta = 1$ for this problem, or in the case of very diffusive regimes, we use the the simple scheme (87).

In the transition regime (Figures 7c-d), profiles for the first two moments of the two methods give very similar results. There are two minor differences: (i) the DG scheme clips

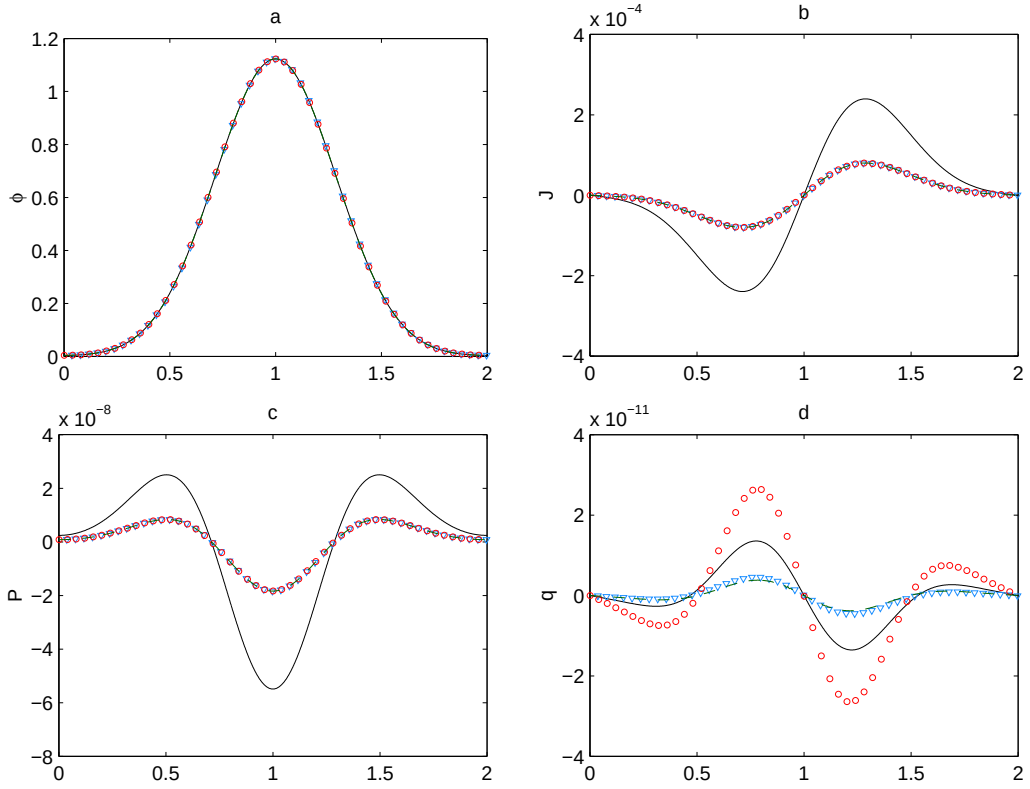

Figure 4: Same case as Fig. 3, but high resolution ($h = 0.002$). Solid line: the upwind scheme with $\Delta t = 0.1\varepsilon h$; circles: DG with $\Delta t = 0.3\varepsilon h$; triangles: regularization with $\Delta t = 0.1h$. The diffusion solution (dashed line) is also plotted but not easily visible due to overlap.

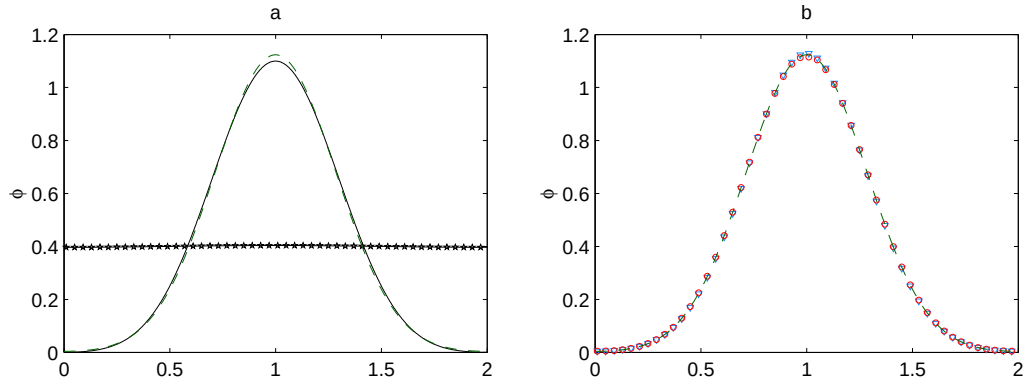

Figure 5: Same case as Fig. 3, but for $\varepsilon = 10^{-6}$; Left: the upwind scheme with $h = 0.02$ (stars) and $h = 0.002$; $\Delta t = 0.1\varepsilon h$. Right: DG scheme (circles) with $\Delta t = 0.3\varepsilon h$ and regularization (triangles) $\Delta t = 0.1h$; in both cases, $h = 0.02$. The diffusion solution (dashed line) is also plotted but not easily visible due to overlap.

the density profile at $x = 1.0$ and (ii) the small discontinuities in the regularized solution for J at $x = 0.65$ and $x = 1.35$ are not present in the DG solution.

In the diffusive regime (Figures 7e-f), we use the simple wave-splitting algorithm (87)

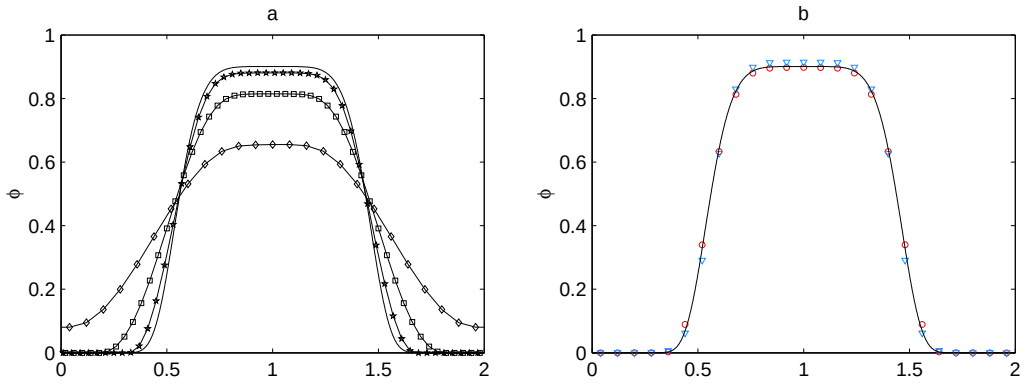

Figure 6: Vanishing cross-section results, with $N = 7$, $\varepsilon = 10^{-3}$, and at $t = 0.1$. Left: upwind results with $h = 0.08$ (diamonds), with $h = 0.04$ (squares), with $h = 0.02$ (stars), and with $h = 0.002$ (no marker). In all cases, $\Delta t = 0.1\varepsilon h$. Right: DG solution (circles) and regularized solution (87) computed using simple wave splitting scheme. In both cases, $h = 0.08$. For DG, $\Delta t = 0.3\varepsilon h$; for the regularization, $\Delta t = 0.1\varepsilon h$. Solid line is the same upwind solution as on the right, with mesh spacing $h = 0.002$.

to compute regularized solutions because (89) is unstable. The profile for ϕ for the DG and regularized solutions agree quite closely, again with only minor differences at $x = 1.0$. However, the DG solution does a much better job capturing the smooth behavior of J. Indeed, by breaking up the term $\gamma B\partial_x(\mathbf{u}^k)$ in (73), we have altered the numerical balance for J and for the other higher order moments, and the effect of our treatment becomes more pronounced as ε becomes smaller. In this case, the main benefit of our implementation is the increased time step allowed by the regularized method whenever ε is under-resolved. Whereas the DG scheme required a time step $\Delta t = 6.0 \times 10^{-8}$ for stability, the regularized method used $\Delta t = 2.0 \times 10^{-3}$ and yet obtained similar accuracy.

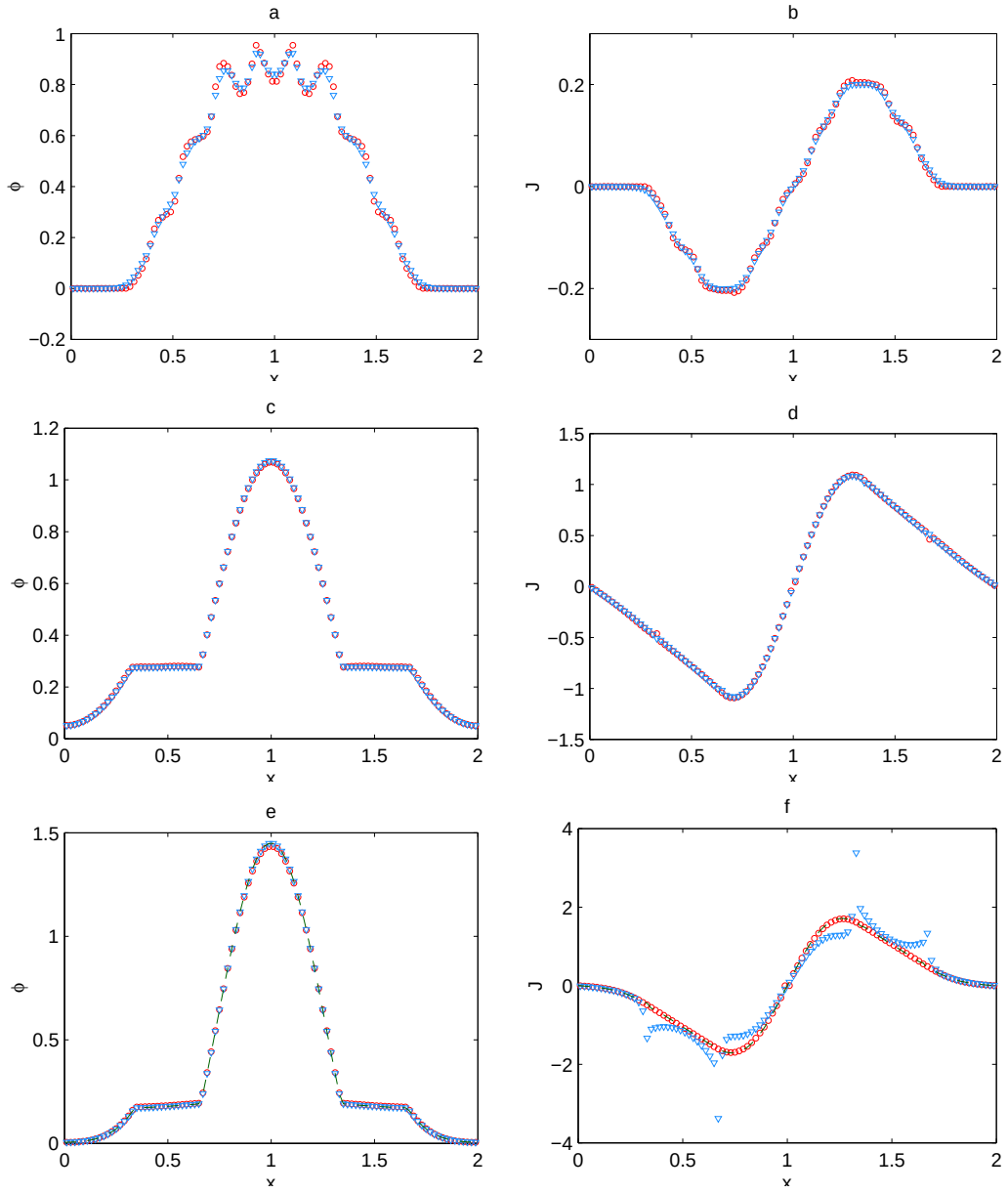

Figure 7: Discontinuous cross-section results, with $N = 7$ and for several values of ε. The left plots are ϕ and right plots are J. From top to bottom: $\varepsilon = 2.0$ and $t = 1.0$; $\varepsilon = 4.0\times10^{-2}$ and $t = 0.1$; $\varepsilon = 10^{-5}$ and $t = 0.05$. In plots (a)-(d), the regularized solution is computed with the wave-splitting scheme and flux corrections (89). In plots (e)-(f), solutions are computed using the simpler scheme (87). The diffusion solution (dashed line) is also given in plots (e)-(f), but is not easily visible due to overlap. All computations use $h = 0.02$. For the DG scheme, $\Delta t = 0.3\varepsilon h$. For the regularized equations, the times steps are (from top to bottom) $\Delta t = 2.0 \times 10^{-3}$, 8.0×10^{-3}, and 2.0×10^{-3}.

7 Discussion and Conclusions

We have presented two very different approaches to address numerical difficulties associated with diffusive relaxation in the P_N equations in the context of a highly simplified neutron transport model. The first method is based on the standard DG formulation and takes advantage of additional local variables in each computational cell to achieve the proper diffusion limit in collision-dominated regimes. The second method uses an operator splitting to derive regularized equations that are more amenable to efficient computation in the diffusion limit. The splitting is based on the balance of terms which lead to the diffusion limit.

Each method studied here has its own advantages and disadvantages. For the DG method, the advantage is its relative simplicity. Unlike the regularization approach (and all other approaches of which we are aware), at least in 1-D, the DG approach requires no special treatment in order to attain the diffusion limit. It should be noted that on certain meshes in multidimensional settings, the standard DG approach must be modified in order to attain the diffusion limit [1]. Another aspect of DG that requires extra care is the method of slope limiting, which for semi-implicit time integration, can be implemented as a post-processing step [44]. At this point, one drawback of the DG approach is that it remains numerically stiff; i.e., the time step is restricted as $O(\varepsilon\Delta t)$, even in the diffusion limit. This problem may be overcome with fully implicit time integration, but at a significant increase in the computational cost per time step. Another disadvantage of DG methods is due to its number of degrees of freedom per spatial cell. For three-dimensional calculations using hexahedral mesh cells, in order to be asymptotic preserving, DG must use trilinear elements which have a factor of eight more unknowns per cell than finite-volume methods [1]. On the other hand, the effective local stencil of DG methods means that their parallel implementation is typically easier than for finite-volume methods.

The regularization approach, coupled with our finite-volume discretization, has the benefit of a large time step in the diffusion limit. If the computational mesh resolves the wave structure of the problem, then this time step corresponds to that of explicit diffusion. When the wave structure is not resolved, an implicit treatment of the diffusion term in the regularized system means that the time step can be set based solely on accuracy requirements. However, the increased time step allowed by the regularization approach is less of an advantage when simulating both diffusive and fully-streaming regimes, as in the vanishing cross-section case given in Sec. 6.1. In such cases, the global time step is restricted by the streaming regime and therefore scales with ε. The major disadvantage of the regularized approach is that the regularized equations have non-conservative terms whose discretization require special care. Indeed, our current implementation of the wave-splitting algorithm has proven to be unstable in some cases and unable to handle properly discontinuities in the cross-section.

Both methods are currently being advanced in several ways. Our formulation of DG has been successfully used for thermal radiative transfer [43]. Current work involves improving the time-step for the semi-implicit method presented here and coupling the method to other physical processes, such as hydrodynamics [38]. Improved spatial discretization of the RP_N equations is also work in progress, as are applications to radiative transfer. In addition, both methods are being extended to handle multi-dimensional problems. Limiter effects in diffusive regimes are also being addressed.

References

[1] M. L. Adams, *Discontinuous finite element transport solutions in thick diffusive problems*, Nucl. Sci. Eng., 137 (2001), pp. 298–333.

[2] M. L. Adams and P. F. Nowak, *Asymptotic analysis of a computational method for time- and frequency-dependent radiative transfer*, J. Comp Phys., 146 (1998), pp. 366–403.

[3] G. B. Arfken and H. J. Weber, *Mathematical Methods for Physicists*, Academic Press, San Diego, 4th ed., 1995.

[4] E. Audusse, F. Bouchut, M.-O. Bristeau, R. Klein, and B. Perthame, *A fast and stable well-balanced scheme with hydrostatic reconstruction for shallow water flows.*, SIAM J. Sci. Comp., 25 (2004), pp. 2050–2065.

[5] D. S. Bale, R. J. Leveque, S. Mitran, and J. . Rossmanith, *A wave propogation method for conservation laws and balance laws with spatially varying flux functions*, SIAM J. Sci. Comp., 24 (2003), pp. 955–978.

[6] G. I. Bell and S. Glasstone, *Nuclear Reactor Theory*, Robert E. Kreiger Publishing, Malabar, Florida, 1970.

[7] F. Bouchut, G. Ounaissa, and B. Perthame, *Upwinding of the source term at interfaces for Euler equations with high friction*, Computers and Mathematics with Applications, 53 (2007), pp. 361–375.

[8] T. A. Brunner and J. P. Holloway, *One-dimensional Riemann solvers and the maximum entropy closure*, J. Quant Spectrosc. Radiat. Transfer, 69 (2001), pp. 543–566.

[9] C. Buet and S. Cordier, *Asymptotic preserving scheme and numerical methods for radiative hydrodynamic models*, C. R. Acad. Sci Paris, Ser. I, 338 (2004), pp. 951–956.

[10] K. M. Case and P. F. Zweifel, *Linear Transport Theory*, Addison-Wesley, Reading, Massachusetts, 1967.

[11] C. Cattaneo, *On the conduction of heat*, Atti Del Seminar. Mat. Fis. Univ., Modena, 3 (1948), pp. 3–21.

[12] ——, *Sur une forme de lequation de la chaleur eliminant le paradoxe dune propagation instantanee*, Comptes Rendus Acad. Sci., 247 (1958), pp. 431 – 433.

[13] C. Cercignani, *The Boltzmann Equation and Its Applications*, Springer-Verlag, New York, 1988.

[14] B. Cockburn and C.-W. Shu, *TVB Runge-Kutta projection discontinuous Galerkin finite element method for conservation laws II: General framework*, Mathematics of Computation, 52 (1989), pp. 411–435.

[15] R. B. DeBar, *Truncation of the spherical harmonic expansion of the transport equation*, Nuclear Science and Engineering, 30 (1967), pp. 159–165.

[16] F. Filbet and B. P. Ph. Lauren¸ot, *Derivation of hyperbolic models for chemosensitive movement*, J. Math. Biol., 50 (2005), pp. 189–2007.

[17] F. Filbet and C.-W. Shu, *Approximation of hyperbolic models for chemosensitive movement*, SIAM J. Sci. Comp., 27 (2005), pp. 850–872.

[18] M. Frank, B. Dubroca, and A. Klar, *Partial closures entropy approximation to radiative heat transfer*, J. Comput. Phys., 218 (2006), pp. 1–18.

[19] S. Goldstein, *On diffusion by discontinuous movements, and on the telegraph equation*, Quart. J. Mech. Appl. Math., 4 (1951), pp. 129–156.

[20] F. Golse and C. Levermore, *Hydrodynamic limits of kinetic models*, Fields Institute Communications, 46 (2005), pp. 1–75.

[21] L. Gosse and G. Toscani, *An asymptotic-preserving, well-balanced scheme for the hyperbolic heat equations*, C. R. Acad. Sci. Paris, Ser. I, 334 (2002), pp. 337–342.

[22] ——, *Asymptotic-preserving and well-balance schemes for radiative transfer and the Rosseland approximation*, Numerische Mathematik, 98 (2004), pp. 223–250.

[23] M. Gurtin and A. C. Pipkin, *A general theory of heat conduction, with finite wave speeds*, Arch. Rational Mech. Anal., 31 (1968), pp. 113–126.

[24] C. D. Hauck, *Entropy-Based Moment Closures in Semiconductor Models*, PhD thesis, University of Maryland, College Park, 2006.

[25] C. D. Hauck and R. B. Lowrie, *Temporal regularization of the P_N equations*, Los Alamos Report LA-UR 07-7995, to appear in SIAM J. Multiscale Modeling and Analysis, (2008).

[26] S. Jin, *Efficient asymptotic preserving (AP) schemes for some multiscale kinetic equations*, SIAM J. Sci. Comp., 21 (1999), pp. 441–454.

[27] S. Jin, L. Pareschi, and G. Toscani, *Diffusive relaxation schemes for multiscale discrete-velocity kinetic equations*, SIAM J. Numer. Anal., 35 (1998), pp. 2405–2439.

[28] ——, *Uniformly accurate diffusive relaxation schemes for multiscale transport equations*, SIAM J. Numerical Analysis, 98 (2000), pp. 913–936.

[29] A. Klar, *An asymptotic-induced scheme for nonstationary transport equations in the diffusive limit*, SIAM J. Num. Anal., 35 (1998), p. 1073.

[30] T. G. Kurtz, *Convergence of sequences of semigroups of nonlinear operators with an application to gas kinetics*, Trans. Amer. Math. Soc., 186 (1973), pp. 259–272.

[31] E. W. Larsen and J. E. Morel, *Asymptotic solutions of numerical transport problems in optically thick, diffusive regimes. ii.*, Journal of Computational Physics, 83 (1989), pp. 212 – 36.

[32] E. W. Larsen, J. E. Morel, and W. F. Miller, *Asymptotic solutions of numerical transport problems in optically thick, diffusive regimes*, J. Comp. Phys., 69 (1987).

[33] P. Lesaint and P.-A. Raviart, *On a finite element method for solving the neutron transport equation*, in Mathematical Aspects of Finite Elements in Partial Differential Equations, C. de Boor, ed., Academic Press, 1974, pp. 89–145.

[34] R. J. LeVeque, *Numerical Methods for Conservation Laws*, Birkhäuser Verlag, Basel, second ed., 1992.

[35] C. D. Levermore, *Relating eddington factors to flux limiters*, J. Quant. Spectrosc. Radiat. Transfer, 31 (1984), pp. 149–160.

[36] E. E. Lewis and J. W. F. Miller, *Computational Methods in Neutron Transport*, John Wiley and Sons, New York, 1984.

[37] P.-L. Lions and G. Toscani, *Diffusive limit for finite velocity Boltzmann kinetic models*, Rev. Mat Iberoamericana, 13 (1997), pp. 473–513.

[38] R. B. Lowrie and J. E. Morel, *Discontinuous Galerkin for hyperbolic systems with stiff relaxation*, in Discontinuous Galerkin Methods: Theory, Computation and Applications, B. Cockburn and G. E. Karniadakis, eds., Springer, 2000, pp. 385–390.

[39] ——, *Methods for hyperbolic systems with stiff relaxation*, Int. J. Numer. Meth. Fluids, 40 (2002), pp. 413–423.

[40] P. Marcati and B. Rubino, *Parabolic relaxation limit for hyperbolic systems of conservation laws*, Proceedings of the VIII conference on Waves and Stability, (1996), pp. 393–406.

[41] ——, *Hyperbolic to parabolic relaxation theory for quasilinear first order systems*, J. Differential Equations, 162 (2000), pp. 359–399.

[42] K. A. Mathews, *On the propagation of rays in discrete ordinates.*, Nuclear science and engineering, 132 (1999).

[43] R. G. McClarren, T. M. Evans, R. B. Lowrie, and J. D. Densmore, *Semi-implicit time integration for P_N thermal radiative transfer*, J. Comp. Phys., 227 (2008), pp. 7561–7586.

[44] R. G. McClarren and R. B. Lowrie, *The effects of slope limiting on asymptotic-preserving numerical methods for hyperbolic conservation laws*, J. Comp. Phys. accepted for publication, (2008).

[45] H. P. McKean, *The central limit theorem for Carlemann's equation*, Israel J. Math, 21 (1975), pp. 54–92.

[46] D. Mihalas and B. Weibel-Mihalas, *Foundations of Radiation Hydrodynamics*, Dover Publications Inc., Mineola, New York, 1999.

[47] G. N. Minerbo, *Maximum entropy Eddington factors*, J. Quant. Spectrosc. Radiat. Transfer, 20 (1978), pp. 541–545.

[48] J. E. Morel, *Diffusion-limit asymptotics of the transport equation, the $P_{1/3}$ equations, and two flux-limited diffusion theories.*, Journal of Quantitative Spectroscopy and Radiative Transfer, 65 (2000), pp. 769 – 78.

[49] G. B. Nagy, O. E. Ortiz, and O. A. Reu, *The behavior of hyperbolic heat equations solutions near their parabolic limits*, J. Math. Phys, 35 (1994), pp. 4344 – 4356.

[50] G. Naldi and L. Pareschi, *Numerical schemes for hyperbolic systems of conservation laws with stiff diffusive relaxation*, SIAM J. Numer. Anal., 37 (2000), pp. 1246–1270.

[51] G. C. Pomraning, *Radiation Hydrodynamics*, Pergamon Press, New York, 1973.

[52] W. H. Reed and T. R. Hill, *Triangular mesh methods for the neutron transport equation*, Tech. Rep. LA-UR-73-479, Los Alamos Scientific Laboratory, 1973.

[53] P. L. Roe, *Characterstic-based schemes for the Euler equations*, Ann. Rev. Fluid Mech., 18 (1986), pp. 337–365.

[54] ——, *Upwind difference schemes for hyperbolic conservation laws with source terms*, in Nonlinear Hyperbolic Problems, C. Carraso, P.-A. Raviart, and D. Serre, eds., vol. 1270 of Lecture Notes in Mathematics, Springer-Verlag, 1986, pp. 41–51.

[55] S.Jin, L.Pareschi, and G. Toscani, *Uniformly accurate diffusive relaxation schemes for multiscale transport equations*, SIAM J. Numer. Anal., 38 (2001), pp. 913–936.

[56] R. P. Smedley-Stevenson, *Single-ray streaming behavior for discontinuous finite element spatial discretizations.*, Nuclear science and engineering, 142 (2002).

[57] Y. Sone, *Kinetic Theory and Fluid Dynamics*, Birkhäuser, Boston, 1988.

[58] G. I. Taylor, *Diffusion by continuous movements*, Proc. London Math. Soc., 20 (1921), pp. 196–212.

[59] B. van Leer, *Towards the ultimate conservative difference scheme IV. A new approach to numerical convection*, Journal of Computational Physics, 23 (1977), pp. 276–299.